

**Minas Liarakis<sup>1</sup>**

School of Engineering and Applied Science,  
Yale University,  
9 Hillhouse Avenue,  
New Haven, CT 06511  
e-mail: minas.liarakis@yale.edu

**Charalampos P. Bechlioulis**

School of Mechanical Engineering,  
National Technical University of Athens,  
Athens 15780, Greece  
e-mail: chmpechl@mail.ntua.gr

**Panagiotis K. Artemiadis**

School for Engineering of Matter,  
Transport and Energy,  
Arizona State University,  
Tempe, AZ 85287  
e-mail: panagiotis.artemiadis@asu.edu

**Kostas J. Kyriakopoulos**

School of Mechanical Engineering,  
National Technical University of Athens,  
Athens 15780, Greece  
e-mail: kkyria@mail.ntua.gr

# Deriving Humanlike Arm Hand System Poses

*Robots are rapidly becoming part of our lives, coexisting, interacting, and collaborating with humans in dynamic and unstructured environments. Mapping of human to robot motion has become increasingly important, as human demonstrations are employed in order to “teach” robots how to execute tasks both efficiently and anthropomorphically. Previous mapping approaches utilized complex analytical or numerical methods for the computation of the robot inverse kinematics (IK), without considering the humanlikeness of robot motion. The scope of this work is to synthesize humanlike robot trajectories for robot arm-hand systems with arbitrary kinematics, formulating a constrained optimization scheme with minimal design complexity and specifications (only the robot forward kinematics (FK) are used). In so doing, we capture the actual human arm-hand kinematics, and we employ specific metrics of anthropomorphism, deriving humanlike poses and trajectories for various arm-hand systems (e.g., even for redundant or hyper-redundant robot arms and multifingered robot hands). The proposed mapping scheme exhibits the following characteristics: (1) it achieves an efficient execution of specific human-imposed goals in task-space, and (2) it optimizes anthropomorphism of robot poses, minimizing the structural dissimilarity/distance between the human and the robot arm-hand systems. [DOI: 10.1115/1.4035505]*

## 1 Introduction

Since the beginnings of robotics, mapping of human to robot motion was necessary for a series of applications that range from teleoperation and telemanipulation studies, to closed-loop, anthropomorphic grasp planning. In particular, the extraction of anthropomorphic robot motion is useful for robots that collaborate, interact, and co-exist with humans in dynamic and/or human-centric environments. Anthropomorphism is derived from the Greek words *anthropos* (human) and *morphe* (form). A robot may be characterized as anthropomorphic or humanlike if it mimics the human form. According to Epley et al. [1], the purpose of anthropomorphism is “to imbue the imagined or real behavior of nonhuman agents with humanlike characteristics, motivations, intentions, and emotions.” Regarding the different classes of anthropomorphism, a clear distinction between functional and perceptual anthropomorphism was recently proposed in Ref. [2]. Functional anthropomorphism has as its first priority to guarantee the execution of a specific functionality in task-space and only after accomplishing such a prerequisite to optimize anthropomorphism of structure (minimizing a “distance” between the human and robot poses). Perceptual anthropomorphism concerns all synergistic motions, behaviors, decisions, and emotions that can be perceived by the humans, as humanlike.

An important question is: why has anthropomorphism become significant and necessary? Nowadays, we experience an increasing demand for human robot interaction (HRI) applications. We believe that anthropomorphism of robot motion is important in these applications as it increases safety in human and robot interactions and facilitates the establishment of a solid social connection between the human and the robots. More precisely, regarding social connection, the more humanlike a robot is in terms of motion, appearance, expressions, and perceived intelligence, the more easily it will manage to create meaningful “relationships” with human beings as robot likeability is increased [3]. Regarding

safety in HRI scenarios, when robots move anthropomorphically, users can more easily predict their motion and comply with their activity, thus avoiding injuries. Gielen et al. [4] support this idea, discussing in their work that: “humanlike motion supports natural human–robot interaction by allowing the human user to more easily interpret movements of the robot in terms of goals. This is also called motion clarity.”

In this respect, anthropomorphism increases robots’ motion expressiveness, which may be critical for scenarios in which humans and robots cooperate advantageously, in order to execute specific tasks. Beetz et al. [5] first elaborated the idea of creating legible and predictable robot motions, while the idea of the legibility of robot motion goes back to Alami et al. [6]. Dragan and Srinivasa [7] proposed a methodology based on gradient optimization techniques for autonomously generating legible robot motion (e.g., motion that communicates its intent to a human observer). More precisely, the proposed algorithm optimizes a legibility metric inspired by the psychology of action interpretation in humans, deriving robot motion trajectories that better express intent. The motivation behind this study comes from the fact that when humans are able to predict the outcome/intent of robot motions, they may comply with their motion and avoid injuries or enhance collaborations. Similarly, deriving anthropomorphic robot motions can be significant not only for aesthetic but also for practical reasons.

Over the last decades, numerous schemes have been proposed that map human to robot hand motion. The most well known methodologies are: (1) the fingertips (point-to-point) mapping, (2) the joint-to-joint (angle-to-angle) mapping, (3) the functional pose mapping, and (4) the object-specific mapping. Fingertips mapping appears in Ref. [8] and is based on the computation of forward and inverse kinematics for each human and robot finger, in order to achieve same fingertip positions in 3D space. The linear joint-to-joint mapping is a one-to-one, angle-to-angle mapping where the joint angle values of the human hand are directly assigned to the corresponding joints of the robot hand [9]. In joint-to-joint mapping, the replicated by the robot postures are identical to the human hand postures, as human and robot finger links attain same orientations. Functional pose mapping [10] places both the human

<sup>1</sup>Corresponding author.

Manuscript received May 30, 2016; final manuscript received December 10, 2016; published online January 9, 2017. Assoc. Editor: Marcia K. O’Malley.

and the robot hand in a number of similar functional poses, and then a relationship between each human and robot joint is found (e.g., using the least squares fit method). Finally, the object-specific mapping [11] provides a mapping approach between the human and robot hand configurations that takes into consideration a specific object to be grasped. In Ref. [12], authors extended the object-based approach, to map synergies from human to robot hands with dissimilar kinematics.

Regarding arm motion mapping, most previous studies focused on a forward-inverse kinematics approach that achieves same position and orientation for human and robot arm end-effectors, without guaranteeing humanlikeness of robot motion. In Ref. [13], neural networks and quadratic programming methods were utilized to solve the inverse kinematics of redundant manipulators. A biomimetic approach for a 7 degrees of freedom (DOF) redundant robotic arm was presented in Ref. [14]. In that study, the authors used human arm motions to describe and model the dependencies among the human joint angles via a Bayesian network. Subsequently, an optimization problem was formulated that utilized the extracted model for the computation of the robot arm's inverse kinematics. Chirikjian and Burdick [15] proposed an inverse kinematics computation method for hyper-redundant robot arms. In Ref. [16], the authors used a control approach for hyper-redundant arms, formulating a constrained optimization problem. In Ref. [17], the process of manipulating the pose of an articulated figure was approached as a nonlinear, constrained optimization problem. Finally, in Ref. [18], the authors proposed a method that solves the inverse kinematics problem of highly articulated figures, utilizing methods of nonlinear programming. It should be noted that although nonlinear programming algorithms may terminate at local minima, the aforementioned studies have inspired numerous researchers over the last years.

Regarding anthropomorphism of robot motion, a recent study [19] focused on the extraction of humanlike robot arm-hand system configurations using a criterion from ergonomics. In Ref. [20], a combination of bio-inspired optimization principles was incorporated in an optimization problem, to compute humanlike robot reaching trajectories. In Ref. [21], a model-free control scheme was proposed that provides humanlike, smooth motion, and compliance properties to redundant arms. In Ref. [22], the authors formulated a nonlinear optimization problem using obstacle constraints between the robot arm-hand system and the environment, in order to generate humanlike movements. In Ref. [23], the authors proposed a methodology for planning the motion of dual-arm anthropomorphic systems, reducing the computational cost of the planning process, and deriving humanlike robot movements. In particular, they adopted the synergies of the dual-arm anthropomorphic system to reduce the dimension of the search space, preserving the humanlikeness of the robot motions. Finally, Gielniak and Thomaz [24] proposed a method for making the robot motion more humanlike, by optimizing with respect to a nonlinear spatiotemporal correspondence (STC) metric for distributed actuators.

In this paper, we propose a generic human to robot motion mapping scheme of low-complexity and computational cost that derives humanlike robot poses and trajectories. The proposed scheme can be employed for any type of robot arms, hands, and robot arm-hand systems and for an arbitrary number of DOF (e.g., redundant or even hyper-redundant robot arms and multifingered robot hands). More specifically, a constrained optimization problem is formulated that (1) achieves certain human-imposed task goals (e.g., same position and orientation for human and robot end-effectors) and (2) derives humanlike robot poses, utilizing certain metrics of anthropomorphism [2,25]. The proposed methodology employs only the forward kinematics of the examined robots and does not require complex inverse kinematics or Jacobian computations. Three geometric metrics are proposed that quantify anthropomorphism of robot poses, assessing structural dissimilarity between human and robot configurations. In particular, human to robot motion mapping is solved for (1) the arm, (2)

the hand, and (3) the overall arm-hand system (considering as end-effectors the robot fingertips). Finally, regarding  $m$ -fingered robot hands (where  $m \neq 5$ ), we assign human thumb fingertip position as a goal position for one of the robot fingers, and we use splines to interpolate between the rest of the human fingertip positions and compute the goal fingertip positions.

The rest of the document is organized as follows: Sec. 2 presents the experimental equipment, the data collection sessions, and the kinematic models, Sec. 3 focuses on the formulation of the mapping scheme as a constrained optimization problem, Sec. 4 validates the efficiency of the proposed methods through extensive simulated and experimental paradigms, and Sec. 5 concludes the paper.

## 2 Apparatus, Data Collection, and Kinematic Models

**2.1 Motion Capture Systems.** To capture the human arm kinematics, the Liberty (Polhemus, Inc., Colchester, VT) magnetic motion capture system was used. It consists of a reference system and four magnetic position sensors. Three of these sensors were placed on the human shoulder, the elbow, and the wrist. The acquisition frequency of this system is 240 Hz, and it provides high accuracy in both position and orientation (0.000762 m and 0.002617 rad, respectively). The human hand kinematics were captured by the CyberGlove II (Cyberglove Systems, San Jose, CA) motion capture system. This dataglove has 22 sensors measuring 20DOF of the human hand and 2DOF of the human wrist. More specifically, the abduction-adduction and flexion-extension of the wrist, the flexion-extension of the proximal, metacarpal, and distal joints of each finger, as well as the abduction between the fingers were measured. The acquisition frequency of the Cyberglove II is 90 Hz, and the nominal accuracy is 0.01745 rad.

**2.2 Kinematic Model of the Human Arm-Hand System.** A 7DOF model that consists of 3DOF for the shoulder (abduction/adduction, flexion/extension, and internal/external rotation), 2DOF for the elbow (flexion/extension and pronation/supination), and 2DOF for the wrist (flexion/extension and abduction/adduction) was adopted for the human arm kinematics. The human hand kinematic model was inspired by the location of Cyberglove II flex sensors. The model of the hand consists of 15 joints and 20DOF. More precisely, for the index, middle, ring, and pinky fingers, we used 3DOF for flexion/extension and 1DOF for abduction/adduction, while for the thumb we adopted 2DOF for flexion/extension, 1DOF for abduction/adduction, and 1DOF to model the opposition. To compute the forward kinematics of the human hand, we need to know the human hand digit lengths and the positions and orientations of the finger base frames. However, in this paper, to diminish the complexity of the proposed methodology, we adopted a set of parametric models derived from hand anthropometry studies [26]. Finally, it should be noted that the proposed methodology can be used with a more sophisticated human hand model, as the one proposed in Ref. [27], in case where all DOF are measurable.

**2.3 Kinematic Models of the Simulated Robot Arm-Hand Systems.** In this subsection, we present the kinematic models of the robot arm-hand systems used in the simulated paradigms. More precisely, we created hyper-redundant robot arms with  $n$ DOF that consist of  $n/3$  spherical joints and  $n/3$  links of equal length. In case that a robot arm is created with  $n$ DOF and  $n$  is not a multiple of three, then the last one or two DOF contribute only to the orientation of the end-effector. In this paper, we created robot arms with 9, 18, 20, 21, 23, 27, and 44 DOF that have a total length less than, equal to, or greater than the mean human arm length (from 80% to 130% of the total length), to prove that our methodology can deal with arbitrary kinematics. Additionally, we adopted as a common human arm length the mean value of the 50th percentile of men and women, as reported in Ref. [28]. Moreover, since

the proposed methodology can be utilized for  $m$ -fingered robot hands with arbitrary number of DOF or phalanges per finger, we also considered three, four, five, and six-fingered robot hands.

Although hyper-redundant robot arms have been an active research topic for the last several decades [15], their applications are still limited in practice. In this work, we considered hyper-redundant robot arms and multifingered hands, to demonstrate that our methodology can deal with arbitrary kinematics. Notice that for such robots the analytical inverse kinematics computation methods fail owing to the multiplicity of their solutions and the complexity involved in their extraction. Thus, constrained optimization schemes are well suited for these robots.

**2.4 Data Collection.** In order to formulate the proposed methodology and validate the efficiency of the proposed methods, two different data collection sessions were held. The first session involved five subjects and focused on offline data collection of human arm-hand system kinematics. The subjects gave informed consent, and the procedures were approved by the Institutional Review Board of the National Technical University of Athens. All subjects performed the experiments with their dominant right arm-hand system. During the experiments, each subject was instructed to perform repeated, random reach to grasp movements in 3D space. During the reach to grasp motions, the subjects were instructed to imagine that they were trying to grasp different objects of different sizes in order to impose a significant variability in the finger trajectories. The first session was used for the initial extraction of the proposed metrics. The second session focused on the real-time teleoperation of simulated robot arm-hand systems and involved only one subject. The second session was used to validate the efficiency of the proposed methods for real-time teleoperation studies. More details regarding the second session can be found in Sec. 4.

**2.5 Mitsubishi PA10-DLR/HIT II Arm-Hand System.** In this paper, we also used a real robot arm-hand system that consists of a Mitsubishi PA10 robot manipulator that has 7DOF and a DLR/HIT II five-fingered robot hand equipped with 15DOF. The Mitsubishi PA10 is a redundant robotic manipulator, which has 2DOF located at the “shoulder,” 2DOF at the “elbow,” and 3DOF located at the “wrist” (end-effector). DLR/HIT II is a dexterous robot hand, jointly developed by German Aerospace Center (DLR) and Harbin Institute of Technology (HIT). DLR/HIT II has five kinematically identical fingers with 3DOF per finger, two for flexion/extension, and one for abduction/adduction. The most distal joint of each finger is mechanically coupled to the middle one, via a steel wire.

### 3 Mapping Human to Robot Motion Methods

In this section, we propose a series of metrics of functional anthropomorphism, and we formulate the mapping of human to robot motion, as a constrained optimization problem that requires only the Denavit-Hartenberg parameters of the robot artifact to solve the robot forward kinematics (no complex IK or Jacobian computation is needed). We have experimentally verified that the problem is well formed (a solution exists even if it is local and the convergence is strong for different initial configurations), and even when the algorithm terminates at a local minimum, the solution suffices for our purposes (typical strategy in related studies [18]). In the sequel, the mapping of human to robot motion is solved for (1) the arm, (2) the hand, and (3) the overall arm-hand system. In all cases, the multiple goals (i.e., position, orientation, and humanlikeness) are combined into a composite objective function, adopting appropriate weight factors. The proposed metrics relate to static poses, and the robot motion is indirectly derived and inherits the temporal characteristics of the human motion.

Task goals (e.g., identical poses for the human and robot end-effectors) are incorporated in the objective function and not

imposed via equality constraints in the optimization problem, since otherwise the problem would probably become infeasible. Such approach allows the user to adjust the position and orientation accuracies by selecting appropriate weights (e.g., high values of the weight of anthropomorphism may favor robot motion humanlikeness during a free space motion, whereas low values may lead in accurate positioning of the robot end-effector).

#### 3.1 Deriving Humanlike Robot Arm Poses

**3.1.1 Position and Orientation Goals.** Let  $\mathbf{x}_{RA} = f_{RA}(\mathbf{q}_{RA})$  denote the forward kinematics mapping from joint to task-space for a robot arm with  $n$ DOF, where  $\mathbf{q}_{RA} \in \mathbb{R}^n$  is the vector of the joint angles, and let  $\mathbf{x}_{RAgoal} \in \mathbb{R}^3$  denote the desired robot end-effector position (i.e., human end-effector position). We may define a metric of success under position goals, as follows:

$$d_{RA_i}(\mathbf{q}_{RA}) = \|\mathbf{x}_{RA} - \mathbf{x}_{RAgoal}\|^2 \quad (1)$$

Let  $\mathbf{h}_c = (a_c, b_c, c_c, d_c)$  and  $\mathbf{h}_g = (a_g, b_g, c_g, d_g)$  denote the current and the desired (i.e., human) end-effector orientation, expressed in the quaternions representation in order to avoid geometric singularities. Their distance in  $\mathbb{S}^3$  is

$$\bar{d}_{RAo}(\mathbf{h}_c, \mathbf{h}_g) = \cos^{-1}(a_c a_g + b_c b_g + c_c c_g + d_c d_g) \quad (2)$$

Hence, considering the antipodal points in  $\mathbb{S}^3$  [29], we propose a proper  $\mathbb{S}^3$  distance metric

$$d_{RAo}(\mathbf{h}_c, \mathbf{h}_g) = \min\{\bar{d}_{RAo}(\mathbf{h}_c, \mathbf{h}_g), \bar{d}_{RAo}(\mathbf{h}_c, -\mathbf{h}_g)\} \quad (3)$$

Thus, a combined metric under position and orientation goals may be defined as follows:

$$F_{RA}^{vo}(\mathbf{q}_{RA}) = w_{RA_i} d_{RA_i}(\mathbf{q}_{RA}) + w_{RAo} d_{RAo}(\mathbf{h}_c, \mathbf{h}_g) \quad (4)$$

where  $w_{RA_i}$  and  $w_{RAo}$  are weights that adjust the relative importance of the position and orientation goals.

**3.1.2 Metrics of Anthropomorphism.** In this subsection, we present a series of geometric metrics of anthropomorphism, which quantify the structural dissimilarity between the human and the robot (see Fig. 1). All the metrics proposed quantify the distance between the human and the robot kinematic chains, if we hypothesize that during the comparison the two chains share a common base frame. This distance relates to (1) the sum of distances between the human and robot joints (metric A), (2) the areas of the possible triangles that can be created by the human and robot joints (metric B), and (3) the volume of the space enclosed between the human and the robot joints that can be approximated with a convex hull/polytope (metric C).

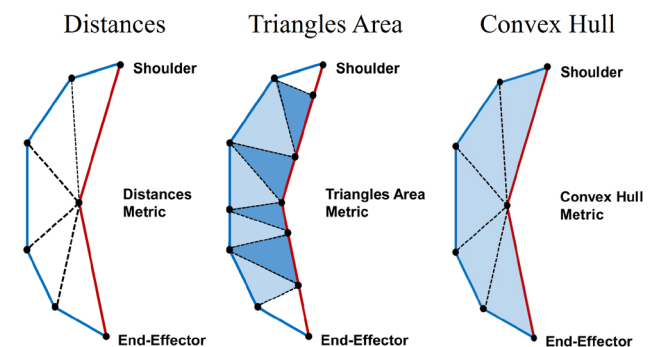


**Fig. 1** Illustrations of the proposed metrics of anthropomorphism. Human arm is the right kinematic chain that consists of two links, while the hypothetical robot arm is the left kinematic chain that has 5 links.

(A) Joint positions distance metric

The metric in this case is the sum of distances between human and robot joint positions in 3D space. For the case of a robot arm, this metric uses the human elbow position as a reference. Hence, let  $s_{\text{elbow}} \in \mathbb{R}^3$  be the position of the human elbow in 3D space, and  $s_j, j = 1, \dots, n$  be the position of each robot joint in 3D space (see Fig. 1). Subsequently, the distance between the robot joints and the human joints (excluding the shoulder and the end-effector) is given by

$$D = \sum_{j=1}^n \|s_{\text{elbow}} - s_j\|^2 \quad (5)$$

(B) Joint positions triangles area metric

Another metric, that quantifies anthropomorphism of robot poses, is the sum of the areas of the triangles defined by the human and robot joints in 3D space. For a  $n$ -link robotic arm, we interpolate extra “virtual” joints in both human and robotic arms, according to the normalized length along their links, from the common base to the end-effector. In this respect, both arms possess equal number of virtual joints, which all have the same normalized length. Selecting one of the arms (e.g., the human arm), we quantify structural dissimilarity/distance as the sum of the areas of all facet triangles that are formed, by joining every internal joint of the human arm (except the common base and the end-effector) with the corresponding and subsequent joint of the robot arm (see Fig. 1). An efficient way to calculate the area of the formed triangles is by employing the Heron’s formula

$$T = \frac{1}{4} \sqrt{(a+b+c)(a-b+c)(a+b-c)(-a+b+c)} \quad (6)$$

where  $a, b$ , and  $c$  are the side lengths of each triangle. The aforementioned metric obtains a minimum value of zero, when all triangle areas are zero and consequently when all triangles vertices are collinear. When the metric reaches its minimum, the human arm coincides with the robot.

(C) Joint positions convex hull volume metric

The third metric, that quantifies anthropomorphism of robot poses, is based on the volume of the convex hulls created by the human and robot joint positions in 3D space. The convex hulls are computed for subsequent subsets of joint positions as depicted in Fig. 1, such that the human shoulder and wrist are not connected. The final volume is the sum of the individual convex hulls volumes. If we include also the line connecting the human shoulder and wrist, then for those robot configurations that lie inside the convex hull (e.g., for a smaller robot arm) the metric has exactly the same value. In the 3D space, the convex hull is the minimal convex polyhedron/polytope that contains all set points. In the general planar case, the convex hull becomes a convex polygon, while when the points lie on a line, the convex hull is the line segment joining the outermost points. Structural dissimilarity once again diminishes, when this metric becomes zero (e.g., human and robot links are coincident). The convex hull of a set of points  $S$  in 3D space is the intersection of all convex sets containing  $S$ . For  $n$  points  $s_1, s_2, \dots, s_n$ , the convex hull  $C$  is defined as follows:

$$C \equiv \left\{ \sum_{k=1}^n a_k s_k : a_k \geq 0 \text{ for all } k \text{ and } \sum_{k=1}^n a_k = 1 \right\} \quad (7)$$

In the 3D case, the volume of a polytope  $P$  is computed via a decomposition into simplices that relies on the volume formula of a simplex. A simplex is a basic geometric element in a Euclidean space and is considered a generalization of the notion of a triangle

or a tetrahedron to arbitrary dimensions. A  $k$ -simplex is a  $k$ -dimensional polytope, thus, a 0-simplex is a point, a 1-simplex is a line, a 2-simplex is a triangle, a 3-simplex is a tetrahedron, etc. The volume formula of a simplex is given by

$$\text{Vol}(\Delta(s_0, \dots, s_n)) = \frac{|\det(s_1 - s_0, \dots, s_n - s_0)|}{n!} \quad (8)$$

where  $\det()$  is the determinant,  $\Delta(s_0, \dots, s_n)$  denotes the simplex in  $\mathbb{R}^n$  with vertices  $s_0, \dots, s_n \in \mathbb{R}^n$ , and each column of the  $n \times n$  determinant is the difference between the vectors representing two vertices ( $v_0, \dots, v_n$ ). When the triangulation method is used for the decompositions, then the volume of  $P$  is simply the sum of the simplices’ volumes

$$\text{Vol}(P) = \sum_{i=1}^N \text{Vol}(\Delta(i)) \quad (9)$$

For the computation of the convex hull, we use the quickhull algorithm [30]. Details regarding the decompositions of the convex hulls and their volumes can be found in Refs. [31] and [32]. Illustrations of the various metrics proposed herein are given in Fig. 1. More detailed results and comparisons of the metrics can be found in Refs. [33] and [34].

**3.1.3 Problem Formulation.** Combining the position/orientation metrics defined in Eq. (4) with any of the proposed metrics of anthropomorphism, we deduce the composite objective function

$$F_{\text{RA}}(\mathbf{q}) = F_{\text{RA}}^{\text{vo}}(\mathbf{q}_{\text{RA}}) + w_A A(\mathbf{q}_{\text{RA}}) \quad (10)$$

where  $w_A$  is the weight that adjusts the relative importance of the anthropomorphic metric, and  $A(\mathbf{q}_{\text{RA}})$  is the value of the selected metric (e.g.,  $A$  is defined either by Eq. (5), (6), or (9)). Hence, the mapping problem is formulated as

$$\text{minimize } F_{\text{RA}}(\mathbf{q}_{\text{RA}}) \quad (11)$$

subject to the inequality constraints of the joints’ limits

$$\mathbf{q}_{\text{RA}}^- < \mathbf{q}_{\text{RA}} < \mathbf{q}_{\text{RA}}^+ \quad (12)$$

where  $\mathbf{q}_{\text{RA}}^-$ ,  $\mathbf{q}_{\text{RA}}^+$  are the lower and upper limits of the joints.

**3.2 Deriving Humanlike Robot Hand Postures.** Having discussed the arm, we now turn to the hand. For an  $m$ -fingered robot hand, let  $\mathbf{x}_{\text{RH}_i} = f_{\text{RH}_i}(\mathbf{q}_{\text{RH}_i})$  be the forward kinematics mapping of the  $i$ th finger with  $n$  DOF, where  $\mathbf{q}_{\text{RH}} \in \mathbb{R}^n$  is the vector of the finger’s joint angles, and let  $\mathbf{x}_{\text{RHgoal}_i} \in \mathbb{R}^3$  denote the corresponding desired fingertip position. Furthermore, let  $d_{\text{RH}o_i}(\mathbf{h}_{c_i}, \mathbf{h}_{g_i})$  denote the distance between the current and the desired orientation (expressed in quaternions) for each robot hand fingertip similarly to Eq. (3). The position, orientation, and anthropomorphism goals may be encapsulated in the following objective function:

$$F_{\text{RH}}(\mathbf{q}_{\text{RH}}) = w_{\text{RHx}} \sum_{i=1}^m \|\mathbf{x}_{\text{RH}_i} - \mathbf{x}_{\text{RHgoal}_i}\|^2 + w_{\text{RH}o} \sum_{i=1}^m d_{\text{RH}o_i}(\mathbf{h}_{c_i}, \mathbf{h}_{g_i}) + w_{\text{RH}a} \sum_{i=1}^m A_i \quad (13)$$

where  $\mathbf{q}_{\text{RH}} \in \mathbb{R}^{m \times n}$  is the vector of the joint angles of the  $m$ -fingered robot hand,  $A_i$  denotes the score of anthropomorphism for each finger (i.e.,  $A_i$  is defined either by Eq. (5), (6), or (9) similarly to the arm case), and  $w_{\text{RHx}}$ ,  $w_{\text{RH}o}$ ,  $w_{\text{RH}a}$  are weights that favor the corresponding goals. Hence, the mapping problem is formulated as follows:

$$\text{minimize } F_{RH}(\mathbf{q}_{RH}) \quad (14)$$

subject to the inequality constraints of joints' limits

$$\mathbf{q}_{RH}^- < \mathbf{q}_{RH} < \mathbf{q}_{RH}^+ \quad (15)$$

where  $\mathbf{q}_{RH}^-$ ,  $\mathbf{q}_{RH}^+$  are the lower and upper limits of the joints, respectively. Moreover, for each finger, we may also adopt equality constraints that encapsulate possible joint couplings.

However, a common robot hand may have less than five fingers [35]. In such case, in order to employ the fingertips mapping methodology [8,36], we first need to define the robot fingertip goal positions. Previous studies used the virtual finger approach [37], computing the virtual fingertip position of a robot hand, as a linear combination of the fingertip positions of the less significant fingers of the human hand (e.g., ring and pinky fingers) [38]. In this paper, we assign human thumb fingertip position as a position goal for one of the robot fingers (the one that we choose to correspond to the human thumb). Subsequently, we use splines<sup>2</sup> to calculate the remaining robot fingertip positions, by interpolating between the other four (index, middle, ring, and pinky) fingertips of the human hand and selecting  $m-1$  equally distant points on the extracted curve (where  $m$  is the number of the robot fingers). Robot thumb (the finger that is chosen to correspond to human thumb) is not taken into account in the fingertips selection procedure, as it should definitely achieve same position and orientation with the human thumb.

*Remark 1.* In this paper, we deal with precision, pinch grasps but the proposed methodology does not assure that the robot hand will grasp the object with a stable, force closure grasp without crushing it. Toward this direction, the proposed methodology could be combined with appropriate controllers that adjust the fingers' stiffness upon contact employing tactile sensing, as discussed in Refs. [39] and [40]. A video presenting such an approach can be found in the footnote below.<sup>3</sup>

**3.3 Deriving Humanlike Robot Arm-Hand Poses.** Typically, the motion of a human arm-hand system may need to be mapped to robots with quite different dimensions in terms of arm link lengths, palm size, finger sizes, phalanges sizes, finger base frames coordinates, etc. Hence, sometimes the solution of the mapping problem may be infeasible. In such cases, however, the dimensional differences may be compensated via a wrist and base offset [2]. In the sequel, we address human to robot motion mapping as a unified optimization problem for the overall arm-hand system. Therefore, we consider the robot fingertips as end-effectors of our system, thus compensating for possible dimensional differences and guaranteeing the execution of specific task goals (e.g., to achieve same position and/or orientation with the human fingertips). The objective function for the arm-hand system is defined as follows:

$$F_{RAH}(\mathbf{q}_{RAH}) = w_{RAHx} \sum_{i=1}^m \|\mathbf{x}_{RAHi} - \mathbf{x}_{RAHgoal_i}\|^2 + w_{RAHo} \sum_{i=1}^m d_{RAHo_i}(\mathbf{h}_{c_i}, \mathbf{h}_{g_i}) + w_{RAH^a} A + w_{RAH^h} \sum_{i=1}^m A_i \quad (16)$$

where  $w_{RAHx}$  and  $w_{RAHo}$  are weights that adjust the relative importance of the position and orientation goals, and  $w_{RAH^a}$ ,  $w_{RAH^h}$  are weights that adjust the relative importance of the anthropomorphic metric for the arm and the hand, respectively. Hence, the mapping problem becomes

<sup>2</sup>Splines are low-degree polynomial functions that are sufficiently smooth at the places where the polynomial curves connect (i.e., knots) and yield smaller errors than linear interpolation.

<sup>3</sup><http://www.youtube.com/watch?v=6jI5d1vaAW8>.

$$\text{minimize } F_{RAH}(\mathbf{q}_{RAH}) \quad (17)$$

subject to the inequality constraints of joints' limits

$$\mathbf{q}_{RAH}^- < \mathbf{q}_{RAH} < \mathbf{q}_{RAH}^+ \quad (18)$$

## 4 Results

In order to verify the efficiency of the proposed methods, both simulated and experimental paradigms are provided. In all cases, the "joint positions distance" metric is used, as it is the most computationally efficient. In order to prepare the simulated paradigms, the MATLAB robotics toolbox [41] was employed. It must be noted that the proposed scheme is of low-complexity and can easily be implemented in real-time, using the C++ based, open-source NLOPT library for nonlinear, constrained optimization [42]. The NLOPT code provides the first solution of the optimization problem in 10 ms and the subsequent solutions at a frequency of 5 kHz (every 0.2 ms). We should also note that we have experimentally verified that the problem is well formed (a solution exists even if it is local and the convergence is strong for different initial configurations). Thus, even when the algorithm terminates at a local minimum, the solution suffices for our purposes. This is a typical strategy in optimization studies [18].

**4.1 Real-Time Teleoperation.** In order to demonstrate the efficiency of the proposed methods in performing in real-time, we conducted different teleoperation experiments. Pictures of the conducted experiments can be found in Fig. 2. The first example (Fig. 2(a)) focuses on the teleoperation of a simulated Mitsubishi PA10-DLR/HIT II robot arm-hand system. The optimization problem was solved online, and a new humanlike robot pose was being derived every 0.2 ms, while the position and orientation tracking errors were always less than 1 mm and 1 deg, respectively (for different poses and terms' weights). The second example focused on the teleoperation of a simulated arm-hand system that consists of a 21DOF robot arm and the DLR/HIT II robot hand. For the hyper-redundant robots, the computation of humanlike robot poses takes more time (10–50 ms). In both cases, the robot arm-hand systems execute the user imposed task goals (e.g., end-effector position and orientation goals), attaining humanlike poses. A video where the proposed scheme is used for real-time teleoperation of the Mitsubishi PA10-DLR/HIT II robot arm-hand system model in the OPENRAVE simulation environment [43] can be found in the footnote below.<sup>4</sup>

**4.2 Autonomous, Anthropomorphic Grasp Planning.** The third example (Fig. 2(c)) involves the Mitsubishi PA10-DLR/HIT II robot arm-hand system performing anthropomorphic reaching and grasping, with humanlike trajectories derived using the proposed mapping scheme. The optimization problem was solved offline for the complete arm-hand system, considering the robot fingertips as the system's end-effectors. A video demonstrating the experiment conducted with the Mitsubishi PA10-DLR/HIT II robot arm-hand system can be found in the footnote below.<sup>5</sup>

**4.3 Comparison of Various Mapping Methodologies.** In this subsection, we present a comparison between different human to robot motion mapping methodologies for the case of the Barrett WAM robot arm. More precisely, the proposed methodology using the joint positions distance metric of anthropomorphism is compared with the "joint-to-joint" mapping and the simple inverse kinematics mapping. Results are depicted in Fig. 3. The proposed methodology derives highly anthropomorphic solutions, while the other two methodologies either do not guarantee the task requirements or result in nonanthropomorphic configurations. More

<sup>4</sup><http://www.youtube.com/watch?v=iKNJTMlcCA>.

<sup>5</sup><http://www.youtube.com/watch?v=wsN23y1oCQQ>.

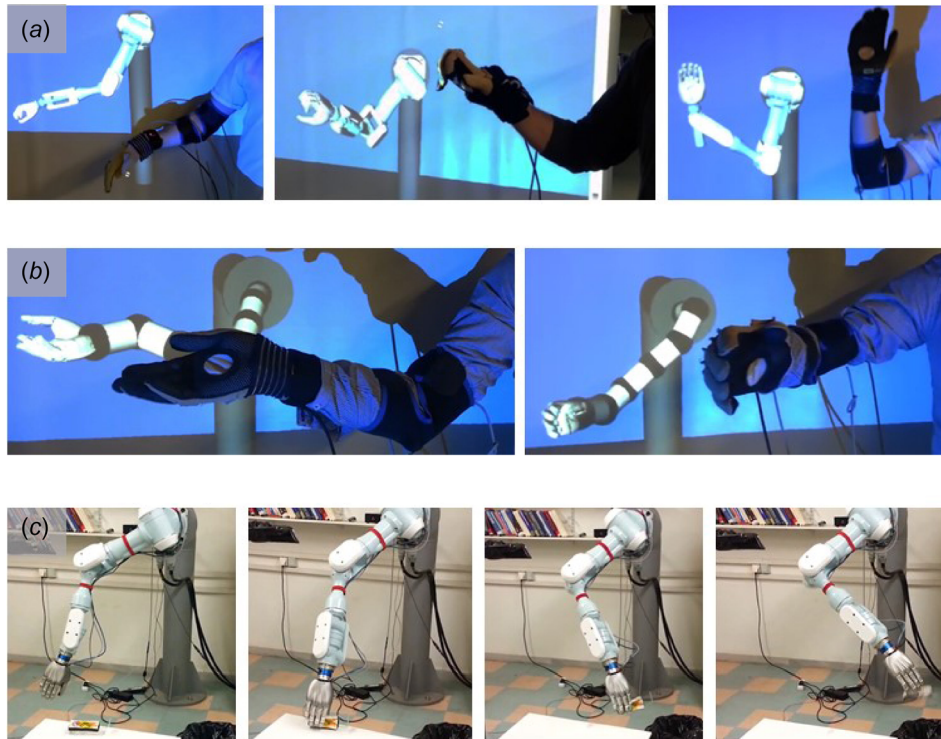


**Fig. 2 Mapping human to robot motion experiments.** The proposed methodology has been used to extract humanlike robot poses for three different applications. (a) The real-time teleoperation of a simulated Mitsubishi PA10-DLR/HIT II arm-hand system. (b) The teleoperation of a simulated arm-hand system that consists of a hyper-redundant robot arm (21DOF) and the DLR/HIT II robot hand. (c) An example of autonomous, anthropomorphic grasp planning using the Mitsubishi PA10-DLR/HIT II arm-hand system.

precisely, the joint-to-joint mapping derives a robot pose that seems humanlike, but the end-effector position tracking error is 66.65 mm (the robot end-effector should have reached the goal position denoted by the gray sphere but it tracks instead only the desired orientation). The inverse kinematics mapping provides excellent trajectory tracking (same position and orientation of the end-effectors) but the poses are typically nonhumanlike.

**4.4 The Case of  $m$ -Fingered Robot Hands.** In this subsection, we focus on  $m$ -fingered hands, in order to demonstrate that the proposed approach can also deal with nontrivial kinematics. Simulated paradigms can be found in Fig. 4. Four simulated paradigms are examined, a hand with three fingers, a hand with four

fingers, an anthropomorphic robot hand with five fingers, and the extreme case of a hand that has six fingers. The desired robot fingertip positions (crosses) are selected from the human fingertip positions (circles) using splines interpolation as discussed in Sec. 3.2. In all cases, the robot hands manage to attain the desired fingertip positions.

In the case of the five-fingered robot hand, the human and robot fingertips attain exactly the same positions. The fingertips position tracking error during the mapping process is less than 1 mm for all

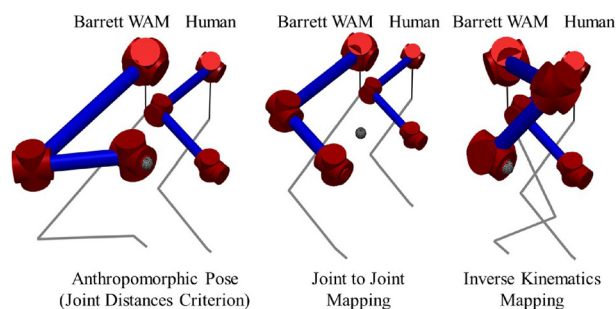


**Fig. 3 Comparison of different mapping methodologies for the case of the Barrett WAM robot arm [44].** The left kinematic chain for all cases is the Barrett WAM robot arm which is longer than human arm (right kinematic chain). The two kinematic chains are depicted with an offset in the  $x$ -axis of their base frames, in order to facilitate comparisons. The sphere denotes the desired end-effector position for the robot arm. For all cases, the human arm pose is the same.

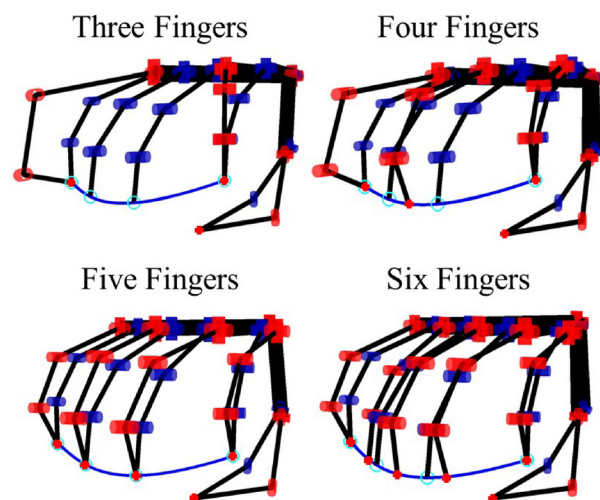


**Fig. 4 Deriving humanlike poses for  $m$ -fingered robot hands with size equal to the 110% of the human hand size.** The selection of the desired robot fingertip positions (crosses) is performed via interpolation between the human fingertip positions (circles).

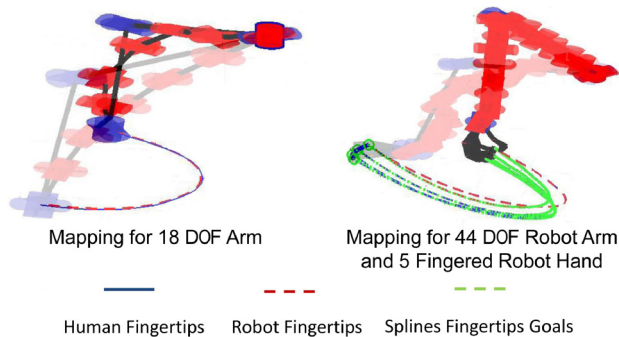


**Fig. 5** Deriving humanlike robot poses for (1) a 18DOF hyper-redundant arm and (2) an arm-hand system that consists of a 44DOF arm and a five-fingered hand

the robot hands examined. It must be noted, though, that the robot fingertips are not able to attain the same orientations with the human fingertips, as they do not have the required redundancy and they are 1.1 times bigger.

**4.5 The Case of Hyper-Redundant Robots.** The proposed methodology can also efficiently derive humanlike robot poses for hyper-redundant arms and arm-hand systems. In Fig. 5, a series of simulated paradigms are presented. More specifically, humanlike robot trajectories are derived for (1) a 18DOF hyper-redundant arm and (2) an arm-hand system that consists of a 44DOF hyper-redundant arm and a five-fingered hand with size equal to the 110% of the human hand size. In all instances, the final configuration appears clearly, while the initial configuration is blurred. In Fig. 6(a), a trajectory tracking example for the end-effector position and orientation of a 20DOF hyper-redundant robot arm executing the human-imposed task goals (i.e., achieve same end-effector position and orientation) is presented. The mean error in position (for all axes) is 0.2 mm, and the mean error in orientation is 0.10 deg. In Fig. 6(b), a trajectory tracking example for the fingertip positions of a hyper-redundant robot arm-hand system is presented. The mean error for all the fingertip positions is less than 1 mm, for all axes and fingers. The fingertips position errors are bigger than those of the arm end-effectors, as typically the robot fingers do not have the kinematic redundancy of the arms that simplifies the tracking problem. More details regarding the effect of the redundancy in the tracking errors can be found in Table 1, where we compare the end-effector position and orientation tracking errors for humanlike trajectories derived by the proposed methodology, for various hyper-redundant arms. More specifically, simulated robot arms with 6, 7, 9, 18, and 27 DOF are considered that have sizes 0.9, 1, 1.15, and 1.3 times the size of the examined human arm. Arms that are smaller than the

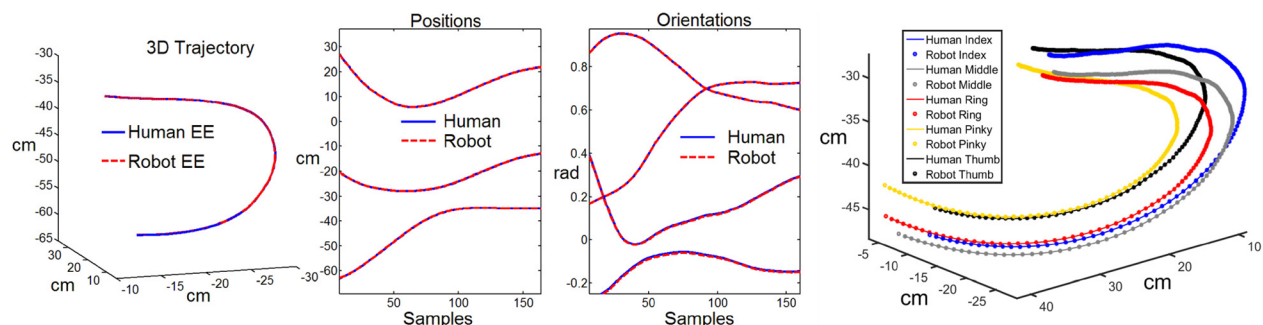


**Fig. 6** (a) A trajectory tracking example that involves a 20DOF hyper-redundant robot arm, the end-effector of which should attain same position and orientation with the human arm end-effector. (b) A trajectory tracking example that involves a hyper-redundant robot arm-hand system that consists of a 23DOF hyper-redundant arm and a five-fingered hand with size equal to the 110% of the human hand size. For this example, the robot fingertips should track the human fingertip positions. The lines denote the human trajectories, and the markers the derived robot trajectories.

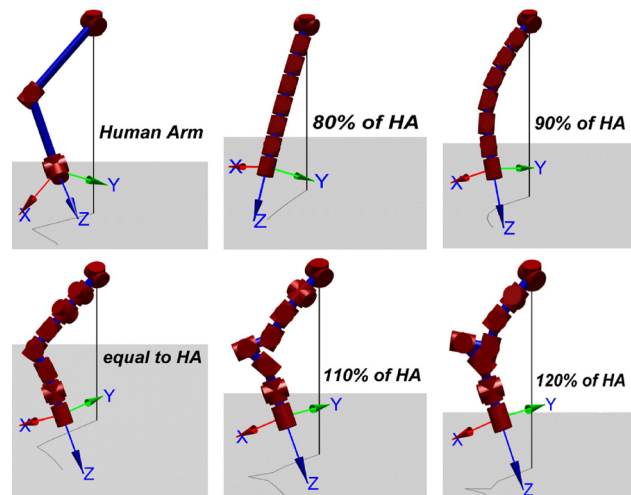


**Fig. 7** Mapping human to robot motion for hyper-redundant robot arms with 21DOF and total length equal to the 80%, 90%, 100%, 110%, and 120% of the total human arm length. HA is the human arm.

**Table 1** End-effector tracking errors ( $p$ —position and  $o$ —orientation) for hyper-redundant robot arms. The scaling factor presents how much bigger than the human arm the robot arm is.

#DOF	$p$ (mm)		$o$ (deg)	
	Scale: 90%		Scale: 100%	
6	0.493	15.5959	0.241	10.9367
7	0.178	13.5371	0.103	9.1192
9	2.430	13.2628	0.021	0.1684
18	2.736	10.6899	0.042	0.1792
27	2.842	8.9306	0.082	0.6010
	Scale: 115%		Scale: 130%	
6	0.152	5.2978	0.007	0.4466
7	0.042	4.1737	0.013	0.2819
9	0.011	0.5697	0.025	1.1485
18	0.030	0.2309	0.022	0.0536
27	0.063	0.2025	0.052	0.1793

human arm have the biggest tracking errors, since they cannot reach the desired position and orientation (the goals may be outside their reachable workspaces). Moreover, an increase in the number of DOF decreases the tracking errors, since redundancy is exploited. In most cases, the position error is less than 1 mm, and the orientation error is less than 1 deg.

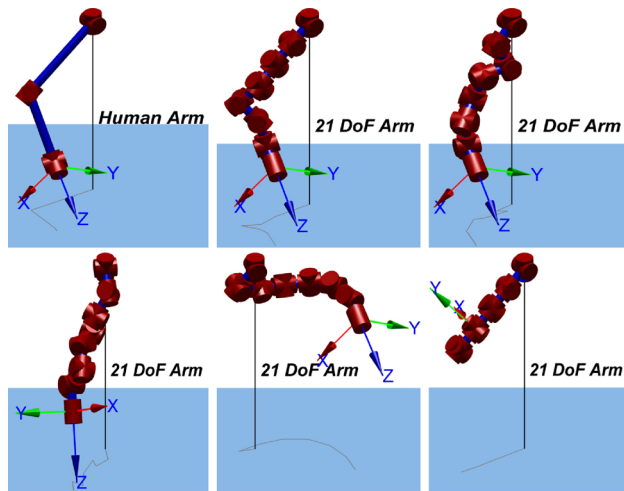


**Fig. 8 Solutions of the mapping problem for a 21DOF robot arm (that has the same length as the human arm) and different terms included in the objective function**

In Fig. 7, we present various examples of mapping human to robot motion for hyper-redundant robot arms with 21DOF and total length equal to the 80%, 90%, 100%, 110%, and 120% of the total human arm length. For the 80% case, the length of the robot arm is not sufficient in order for our scheme to achieve both the position and the orientation goals, while for the 90% case there is a significant error in the derived orientation, caused once again by the size limitations. These results are in accordance with the tracking errors presented in Table 1, as these errors increase for robot arms that are smaller than the human arm. For example, a 27DOF arm with total length 0.9 times the length of the human arm has more than 2 mm end-effector position tracking error and more than 8 deg orientation tracking error, while a 27DOF arm with a total length 1.3 times the human arm length has tracking errors 50 times smaller in position (less than 0.1 mm) and orientation (less than 1 deg).

**4.6 Effect of Optimization Terms.** As we have already noted, in this work, task goals (e.g., identical positions and orientations for the human and robot end-effectors) are incorporated in the objective function instead of being imposed as equality constraints, since otherwise the problem would become infeasible. By doing this, we allow the user to adjust the position and orientation accuracies by selecting appropriate weights. For example, high values of the weight of the score of anthropomorphism may favor humanlikeness of robot motion during a free space movement, whereas low values may lead in accurate positioning of the robot end-effector during tasks that require accuracy (e.g., telemanipulation). In this subsection, we focus on the evaluation of the effect of the different optimization terms in the derived solutions. In Fig. 8, we present various “extreme” solutions of the optimization problem adopting various combinations of the involved terms. A hyper-redundant robot arm with 21DOF is considered. By employing all the terms, the derived configuration is humanlike, and the end-effector achieves same position and orientation with the human arm end-effector (wrist). When only the position and/or orientation terms are used, then the derived configurations are typically nonhumanlike, but the robot’s end-effector achieves small tracking errors. When only the anthropomorphism term is used, all the robot joints are positioned near the human elbow in order to minimize their distance from it. This example is provided only for completeness, as in practice we would never use the metric of anthropomorphism alone.

## 5 Discussion and Conclusions

In this paper, we proposed a generic methodology of low-complexity for deriving humanlike robot trajectories and poses,

even for robot arm-hand systems with arbitrary kinematics. The methodology requires only the Denavit-Hartenberg parameters of the examined robots (to compute their forward kinematics), and no complex inverse kinematics or Jacobian computation is necessary. The problem was formulated, as a constrained optimization problem incorporating in the objective function various metrics of functional anthropomorphism. In particular, three geometric metrics were proposed, which are minimized when the structural dissimilarity between the human and the robotic artifact diminishes. The formulated approach guarantees the execution of specific human-imposed task goals (e.g., same position and orientation for the human and robot end-effectors), optimizing at the same time the humanlikeness of robot poses. The proposed scheme can be used for various HRI applications that require anthropomorphism, ranging from learn by demonstration for autonomous grasp planning, to teleoperation and telemanipulation studies with robot arm-hand systems.

## References

- [1] Epley, N., Waytz, A., and Cacioppo, J., 2007, “On Seeing Human: A Three-Factor Theory of Anthropomorphism,” *Psychol. Rev.*, **114**(4), pp. 864–886.
- [2] Liarakakis, M. V., Artemiadis, P. K., and Kyriakopoulos, K. J., 2012, “Functional Anthropomorphism for Human to Robot Motion Mapping,” 21st IEEE International Symposium on Robot and Human Interactive Communication (RO-MAN), Paris, Sept. 9–12, pp. 31–36.
- [3] Duffy, B. R., 2003, “Anthropomorphism and the Social Robot,” *Rob. Auton. Syst.*, **42**(3), pp. 177–190.
- [4] Gielniak, M. J., Liu, C. K., and Thomaz, A. L., 2013, “Generating Human-Like Motion for Robots,” *Int. J. Rob. Res.*, **32**(11), pp. 1275–1301.
- [5] Beetz, M., Stulp, F., Esden-Tempski, P., Fedrizzi, A., Klank, U., Kresse, I., Maldonado, A., and Ruiz, F., 2010, “Generality and Legibility in Mobile Manipulation,” *Auton. Rob.*, **28**(1), pp. 21–44.
- [6] Alami, R., Clodic, A., Montreuil, V., Sisbot, E. A., and Chatila, R., 2006, “Toward Human-Aware Robot Task Planning,” *AAAI Spring Symposium: To Boldly Go Where No Human-Robot Team Has Gone Before*, pp. 39–46.
- [7] Dragan, A., and Srinivasa, S., 2013, “Generating Legible Motion,” *Robotics: Science and Systems*, Berlin, June.
- [8] Speeter, T. H., 1992, “Transforming Human Hand Motion for Telemanipulation,” *Presence: Teleoper. Virtual Environ.*, **1**(1), pp. 63–79.
- [9] Ciocarlie, M., Goldfeder, C., and Allen, P., 2007, “Dimensionality Reduction for Hand-Independent Dexterous Robotic Grasping,” *IEEE/RSJ International Conference on Intelligent Robots and Systems (IROS)*, San Diego, CA, Oct. 29–Nov. 2, pp. 3270–3275.
- [10] Pao, L., and Speeter, T., 1989, “Transformation of Human Hand Positions for Robotic Hand Control,” *IEEE International Conference on Robotics and Automation (ICRA)*, Scottsdale, AZ, May 14–19, Vol. 3, pp. 1758–1763.
- [11] Griffin, W. B., Findley, R. P., Turner, M. L., and Cutkosky, M. R., 2000, “Calibration and Mapping of a Human Hand for Dexterous Telemanipulation,” *ASME IMECE Symposium on Haptic Interfaces for Virtual Environments and Teleoperator Systems*, pp. 1–8.
- [12] Gioioso, G., Salvietti, G., Malvezzi, M., and Prattichizzo, D., 2013, “Mapping Synergies From Human to Robotic Hands With Dissimilar Kinematics: An Approach in the Object Domain,” *IEEE Trans. Rob.*, **29**(4), pp. 825–837.
- [13] Toshih, H., and Farrokhi, M., 2014, “Real-Time Inverse Kinematics of Redundant Manipulators Using Neural Networks and Quadratic Programming: A Lyapunov-Based Approach,” *Rob. Auton. Syst.*, **62**(6), pp. 766–781.
- [14] Artemiadis, P. K., Katsiaris, P. T., and Kyriakopoulos, K. J., 2010, “A Biometric Approach to Inverse Kinematics for a Redundant Robot Arm,” *Auton. Rob.*, **29**(3–4), pp. 293–308.
- [15] Chirikjian, G., and Burdick, J., 1995, “Kinematically Optimal Hyper-Redundant Manipulator Configurations,” *IEEE Trans. Rob. Autom.*, **11**(6), pp. 794–806.
- [16] Fromherz, M. P. J., and Jackson, W., 2000, “Predictable Motion of Hyper-Redundant Manipulators Using Constrained Optimization Control,” *International Conference on Artificial Intelligence (IC-AI)*, Las Vegas, June 21–26, pp. 1141–1147.
- [17] Engell-Nørregård, M., and Erleben, K., 2011, “A Projected Back-Tracking Line-Search for Constrained Interactive Inverse Kinematics,” *Comput. Graphics*, **35**(2), pp. 288–298.
- [18] Zhao, J., and Badler, N. I., 1994, “Inverse Kinematics Positioning Using Non-linear Programming for Highly Articulated Figures,” *ACM Trans. Graphics*, **13**(4), pp. 313–336.
- [19] Zacharias, F., Schlette, C., Schmidt, F., Borst, C., Rossmann, J., and Hirzinger, G., 2011, “Making Planned Paths Look More Human-Like in Humanoid Robot Manipulation Planning,” *IEEE International Conference on Robotics and Automation (ICRA)*, Shanghai, May 9–13, pp. 1192–1198.
- [20] Albrecht, S., Ramirez-Amaro, K., Ruiz-Ugalde, F., Weikersdorfer, D., Leibold, M., Ulbrich, M., and Beetz, M., 2011, “Imitating Human Reaching Motions Using Physically Inspired Optimization Principles,” *IEEE-RAS International Conference on Humanoid Robots (Humanoids)*, Bled, Slovenia, Oct. 26–28, pp. 602–607.
- [21] Atawneh, A., Papageorgiou, D., and Doulgeri, Z., 2014, “Reaching for Redundant Arms With Human-Like Motion and Compliance Properties,” *Rob. Auton. Syst.*, **62**(12), pp. 1731–1741.

- [22] e Silva, E. C., Costa, F., Bicho, E., and Erlhagen, W., 2011, "Nonlinear Optimization for Human-Like Movements of a High Degree of Freedom Robotics Arm-Hand System," International Conference on Computational Science and its Applications—Volume Part III (ICCSA), pp. 327–342.
- [23] Suárez, R., Rosell, J., and Garcia, N., 2015, "Using Synergies in Dual-Arm Manipulation Tasks," IEEE International Conference on Robotics and Automation (ICRA), Seattle, WA, May 26–30, pp. 5655–5661.
- [24] Gielniak, M. J., and Thomaz, A. L., 2011, "Spatiotemporal Correspondence as a Metric for Human-Like Robot Motion," Sixth International Conference on Human-Robot Interaction (ACM/IEEE), Lausanne, Switzerland, Mar. 6–9, pp. 77–84.
- [25] Liarokapis, M., Artemiadis, P., and Kyriakopoulos, K., 2013, "Mapping Human to Robot Motion With Functional Anthropomorphism for Teleoperation and Telemanipulation With Robot Arm Hand Systems," IEEE/RSJ International Conference on Intelligent Robots and Systems (IROS), Tokyo, Nov. 3–8, p. 2075.
- [26] Pitarch, E. P., 2007, "Virtual Human Hand: Grasping Strategy and Simulation," Ph.D. thesis, Universita Politecnica de Catalunya, Barcelona, Spain.
- [27] Liarokapis, M., Artemiadis, P., and Kyriakopoulos, K., 2013, "Quantifying Anthropomorphism of Robot Hands," IEEE International Conference on Robotics and Automation (ICRA), Karlsruhe, Germany, May 6–10, pp. 2041–2046.
- [28] Poston, A., 2000, *Human Engineering Design Data Digest: Human Factors Standardization Systems/Human Factors Standardization SubTAG*, The Group, Washington, DC.
- [29] LaValle, S. M., 2006, *Planning Algorithms*, Cambridge University Press, Cambridge, UK.
- [30] Barber, C. B., Dobkin, D. P., and Huhdanpaa, H., 1996, "The Quickhull Algorithm for Convex Hulls," *ACM Trans. Math. Software*, **22**(4), pp. 469–483.
- [31] Lawrence, J., 1991, "Polytope Volume Computation," *Math. Comput.*, **57**(195), pp. 259–271.
- [32] Bueler, B., Enge, A., and Fukuda, K., 1997, "Exact Volume Computation for Polytopes: A Practical Study," *Polytopes—Combinatorics and Computation*, Springer, Basel, pp. 131–154.
- [33] Liarokapis, M. V., Artemiadis, P. K., Bechlioulis, C. P., and Kyriakopoulos, K. J., 2013, "Directions, Methods and Metrics for Mapping Human to Robot Motion With Functional Anthropomorphism: A Review," School of Mechanical Engineering, National Technical University of Athens.
- [34] Liarokapis, M. V., 2014, "EMG Based Interfaces for Human Robot Interaction in Structured and Dynamic Environments," Ph.D. thesis, National Technical University of Athens, Athens, Greece.
- [35] Townsend, W., 2000, "The Barrethand Grasper-Programmably Flexible Part Handling and Assembly," *Ind. Rob.: Int. J.*, **27**(3), pp. 181–188.
- [36] Hong, J., and Tan, X., 1989, "Calibrating a VPL Dataglove for Teleoperating the Utah/MIT Hand," IEEE International Conference on Robotics and Automation (ICRA), Scottsdale, AZ, May 14–19, Vol. 3, pp. 1752–1757.
- [37] Arbib, M., Iberall, T., and Lyons, D., 1985, "Coordinated Control Programs for Movements of the Hand," *Hand Function and the Neocortex*, Goodwin, A. W. and Darian-Smith, I., eds., Springer-Verlag, Berlin Heidelberg, pp. 111–129.
- [38] Liu, J., and Zhang, Y., 2007, "Mapping Human Hand Motion to Dexterous Robotic Hand," IEEE International Conference on Robotics and Biomimetics (ROBIO), Sanya, China, Dec. 15–18, pp. 829–834.
- [39] Boutselis, G., Bechlioulis, C., Liarokapis, M., and Kyriakopoulos, K., 2014, "An Integrated Approach Towards Robust Grasping With Tactile Sensing," IEEE International Conference on Robotics and Automation (ICRA), Hong Kong, May 31–June 7, pp. 3682–3687.
- [40] Boutselis, G., Bechlioulis, C., Liarokapis, M., and Kyriakopoulos, K., 2014, "Task Specific Robust Grasping for Multifingered Robot Hands," IEEE/RSJ International Conference on Intelligent Robots and Systems (IROS), Chicago, Sept. 14–18, pp. 858–863.
- [41] Corke, P., 2007, "MATLAB Toolboxes: Robotics and Vision for Students and Teachers," *IEEE Rob. Autom. Mag.*, **14**(4), pp. 16–17.
- [42] Johnson, S. G., 2013, "The NLOpt Nonlinear-Optimization Package," <http://ab-initio.mit.edu/nlopt>
- [43] Diankov, R., and Kuffner, J., 2008, "Openrave: A Planning Architecture for Autonomous Robotics," Robotics Institute, Pittsburgh, PA, *Technical Report No. CMU-RI-TR-08-34*.
- [44] Smith, F., and Rooks, B., 2006, "The Harmonious Robot," *Ind. Rob.: Int. J.*, **33**(2), pp. 125–130.